



Titanium isotopic evidence for a shared genetic heritage of refractory inclusions from different carbonaceous chondrites

Jan Render^{*}, Samuel Ebert, Christoph Burkhardt, Thorsten Kleine
Gregory A. Brennecka

Institut für Planetologie, University of Münster, Wilhelm-Klemm-Str. 10, 48149 Münster, Germany

Received 8 December 2018; accepted in revised form 6 March 2019; Available online 14 March 2019

Abstract

Insights into the earliest stages of our Solar System can be derived from its oldest dated solids, calcium-aluminum-rich inclusions (CAIs). In particular, investigating isotopic anomalies of nucleosynthetic origin in CAIs offers potential clues to the genetic heritage of refractory inclusions and the reservoir(s) involved in their formation. To this point, however, nucleosynthetic anomalies in refractory inclusions have almost exclusively been recognized in (1) relatively large CAIs from CV3 chondrites, employing chemical purification and high-precision mass spectrometry, or (2) from sub-mm-sized hibonite-rich objects (*e.g.*, PLACs, SHIBs) from the Murchison CM2 chondrite using much less precise *in-situ* techniques. Whereas the latter have been shown to be highly anomalous in their isotopic compositions, their genetic connection to ‘regular’ CAIs from carbonaceous chondrites remains poorly understood.

Here, we aim to address this issue by taking advantage of a new technique that allows for high-precision analysis of sub-mm-sized inclusions. Using this method, we report Ti isotope anomalies in a suite of twelve CAIs from five different CO carbonaceous chondrites, as well as ten refractory inclusions from the CM2 chondrite Jbilet Winselwan using MC-ICPMS. We find that these CO and CM CAIs exhibit Ti isotopic compositions very similar to those of previously investigated CV3 (and of two CK3) CAIs, suggesting a fundamental genetic relationship of CAIs found within these chondrite groups. As such, our data indicates that CAIs from various groups of carbonaceous chondrites formed from similar matter and in a single region of the solar nebula (*i.e.*, derived from a single common CAI-formation region). Collectively, these data show evidence of large-scale transport of CAIs over a significant range of heliocentric distances, covering at least the accretion areas of the CV, CK, CO, and CM chondrites. In addition, we report two inclusions consisting of hibonite-rich crystal aggregates from Jbilet Winselwan that exhibit highly irregular nucleosynthetic Ti signatures, implying a distinct origin from the aforementioned CAIs. These inclusions may represent an earlier generation of refractory material, perhaps more akin to the previously mentioned PLACs and/or SHIBs.

© 2019 Elsevier Ltd. All rights reserved.

Keywords: Refractory inclusions; Titanium; Nucleosynthetic isotopic anomalies; CO chondrites; CM chondrites; Early solar system

1. INTRODUCTION

Calcium-aluminum-rich inclusions (CAIs) are assemblages of refractory minerals found in chondritic mete-

orites, interplanetary dust particles, and comets. As the oldest dated solids of the Solar System (*e.g.*, [Connelly et al., 2017](#)), CAIs are prime samples to investigate the beginnings of our stellar system. Furthermore, understanding the origin and distribution of CAIs among Solar System materials is of paramount importance for models of accretion disk dynamics (*e.g.*, [Desch et al., 2018](#)). However, the

^{*} Corresponding author.

E-mail address: jan.render@uni-muenster.de (J. Render).

broad category of CAIs encompasses several subgroups with variable textural, mineralogical, and chemical appearances that are unequally distributed among the different classes and groups of chondritic meteorites, and whose genetic affiliations remain enigmatic.

In recent decades, significant progress regarding the understanding of early Solar System reservoirs has been made by investigations into the isotopic compositions of extraterrestrial materials. For example, it has been shown that CAIs from various chondritic meteorites exhibit similar inferred abundances of the short-lived radionuclide ^{26}Al (e.g., Russell et al., 1996; Jacobsen et al., 2008; Matzel et al., 2013; Ushikubo et al., 2017), however, the uniform distribution of ^{26}Al throughout the protoplanetary disk remains controversial (e.g., Larsen et al., 2011; Wasserburg et al., 2012). Assuming that ^{26}Al was homogeneously distributed throughout the early solar nebula, previous data from CAIs implies their formation within a relative short window of time (≤ 0.3 Myr), regardless of chondrite group. Additionally, refractory inclusions tend to be enriched in ^{16}O compared to almost all other Solar System materials (e.g., McKeegan et al., 1998; Wasson et al., 2001; Itoh et al., 2004; Clayton, 2008; Matzel et al., 2013; Jacobsen et al., 2014; Ushikubo et al., 2017). However, the origin and extent of oxygen isotope heterogeneity in the early Solar System is not yet fully understood (e.g., Krot et al., 2010), and thus using O isotopes to assign genetic relationships between CAIs is not straightforward. In contrast, investigating isotopic anomalies of clear nucleosynthetic origin allows for constraining the genetics of extraterrestrial materials, since these isotope variations fingerprint their source reservoir and, at least for refractory elements, are likely to retain their primordial signature (e.g., Niemeier, 1988; Gerber et al., 2017).

Precise genetic fingerprinting using isotopic anomalies requires sufficient material, and thus becomes more difficult when the object of interest occurs only in sub-mm sizes, as is the case for many CAIs outside of the group of CV meteorites. This analytical challenge has led to an overwhelming research bias (Table 1) towards large CAIs from meteorites of the CV group (and in particular from the widely available Allende meteorite), as these CAIs tend to have the highest abundances and largest sizes of refractory inclusions. Consequently, the nucleosynthetic isotope signatures of CAIs from chondrite groups other than CVs remain largely unexplored, and this prolonged bias begs the question whether relatively large refractory inclusions from CV chondrites are actually representative for, and related to, sub-mm-sized CAIs from other chondritic meteorites.

This issue has been partially addressed by a series of *in-situ* studies employing secondary ion mass spectrometry (SIMS) to investigate isotopic signatures of major elements (i.e., Ca, Ti) in a different type of small-sized, hibonite-rich refractory inclusions, mostly from the Murchison CM2 chondrite (e.g., Ireland, 1990; Liu et al., 2009; Kööp et al., 2016a,b, 2018a; Simon et al., 2019). These combined studies found that spinel-hibonite inclusions (*SHIBs*) derived from a reservoir that was relatively well-mixed with respect to Ca and Ti isotopes, whereas platy hibonite crystals (*PLACs*) can exhibit huge isotopic variations of nucleosynthetic origin for these elements, reaching percent-level deviations from terrestrial (and bulk meteorite) isotopic ratios.

In contrast, previously investigated “regular CAIs” (i.e., excluding those exceptionally rich in hibonite and FUN CAIs), from CV chondrites have a much more restricted range of nucleosynthetic isotope anomalies ($\leq 0.2\%$ relative to terrestrial values, Dauphas and Schauble, 2016), which cannot be resolved with current *in situ* techniques. Due to the precision required to resolve the anomalies present in regular CAIs, investigation of nucleosynthetic isotope anomalies in these samples requires larger amounts of material and different analytical protocols to achieve the necessary precision. Recent improvements, particularly in multi-collector inductively coupled plasma mass spectrometry (MC-ICPMS), allow for investigation of nucleosynthetic isotope anomalies in sub-centimeter-sized meteoritic inclusions.

If the element of interest is abundant enough, this threshold can be reduced to <1 mm (e.g., Gerber et al., 2017; Davis et al., 2018; Larsen et al., 2018; Ebert et al., 2018). In CAIs, this condition is met for the refractory high-field strength element titanium (Ti), which is usually present at the wt% level. Because Ti has five stable isotopes (^{46}Ti , ^{47}Ti , ^{48}Ti , ^{49}Ti , and ^{50}Ti) that are formed in various nucleosynthetic environments, Ti isotopes can potentially provide information about the origin of nucleosynthetic isotope anomalies in CAIs, and the relationships of CAIs from diverse host meteorites.

Previous MC-ICPMS investigations of the Ti isotopic composition of large CAIs from CV chondrites consistently reported excesses in the neutron-rich isotope ^{50}Ti with a range from about 2 to 14 ϵ (parts per ten thousand deviation relative to terrestrial $^{50}\text{Ti}/^{47}\text{Ti}$ after internal normalization) and a peak at around 9 ϵ (e.g., Trinquier et al., 2009; Davis et al., 2018). Recently, Torrano et al. (2017) reported comparable nucleosynthetic Ti isotope anomalies of two CAIs

Table 1
Previously available nucleosynthetic Ti isotope data for CAIs from various chondrite groups (references given in the text).

host chondrite class	# of CAIs investigated	
	regular CAIs (MC-ICPMS)	hibonite-rich objects (in-situ techniques)
CV	>100	3
CK	2	–
CO	2	3
CM	–	>75
CR	–	3
Ordinary chondrites	6	–
Enstatite chondrites	–	–

from CK chondrites, suggesting a close genetic relationship to CV CAIs. This observation is further bolstered by a multi-element isotope study of the same two CK CAIs (Shollenberger et al., 2018a). In addition, Ebert et al. (2018) revealed that six CAIs from ordinary and two CAIs from CO chondrites exhibit $\epsilon^{50}\text{Ti}$ anomalies comparable to those from CV meteorites, suggesting that CAIs from these meteorite groups are similarly genetically linked (Ebert et al., 2018).

Whereas similar $\epsilon^{50}\text{Ti}$ signatures may hint at a similar source, a more useful tool for understanding the genetic relationships of regular CAIs is the correlation of $\epsilon^{50}\text{Ti}$ with the less pronounced anomalies in $\epsilon^{46}\text{Ti}$. This correlation has similarly been observed in bulk Solar System materials and has been ascribed to thermal processing of multiple presolar carrier phases in the protoplanetary disk (Trinquier et al., 2009; Zhang et al., 2011) alongside with the variable incorporation of CAIs or CAI-like material in different bodies (Gerber et al., 2017). Intriguingly, such a correlation between $\epsilon^{46}\text{Ti}$ and $\epsilon^{50}\text{Ti}$ is not observed in single PLAC crystals (Kööp et al., 2016a), but at the current level of analytical uncertainty, could neither be confirmed nor excluded in SHIBs (Kööp et al., 2016b; 2018a). As such, the coherence of anomalies in different Ti isotopes could serve as a useful feature in distinguishing the disparate CAI-subgroups from one another. For instance, if regular CAIs from meteorites other than the CV group formed collectively with those found in CV chondrites, similar enrichments in ^{50}Ti , together with correlated anomalies in ^{46}Ti are expected. This relationship could, in turn, be used to place critical constraints on our understanding of early Solar System dynamics. If regular CAIs with similar nucleosynthetic signatures, such as restricted anomalies ($\leq 20\epsilon$) and correlated Ti isotope anomalies, are present in many types of chondrites, this implies that regular CAIs were formed in a restricted region and subsequently dispersed throughout the protoplanetary disk at various heliocentric distances. Alternatively, if the majority of CAIs found in CM chondrites are genetically related to PLACs and SHIBs (which are most commonly found in CM chondrites, see Table 1), it would suggest that refractory materials found in the CM accretion region have a shared provenance, and one that is very different from CAIs found in other chondrite groups. These two scenarios have very different implications for early Solar System dynamics, but are testable. Here we investigate Ti isotopic compositions of an extensive set of CAIs from the CO and CM chondrite groups to address early large-scale dynamics as one of the Solar System's fundamental characteristics.

2. SAMPLES

The CAIs investigated in this study were identified and characterized from incompletely polished meteorite chips using a JEOL 6610-LV SEM with attached EDX system at the University of Münster. All meteorite samples from which CAIs were extracted and analyzed in this work were provided by the Institut für Planetologie at the University of Münster.

The CAI samples investigated here are listed in Table 2. Detailed information regarding the operating conditions of the electron microscopes, as well as backscattered electron images of selected samples are located in the EA (A1). In order to examine the precision and accuracy of our analytical methods, this sample set was accompanied by the USGS rock standards BCR-2 and BHVO-2, as well as an internal laboratory CAI sample *Egg-2 high* (a mineral separate of high magnetic susceptibility from the Egg-2 Allende CAI, previously reported in Ebert et al. (2018)).

2.1. CAIs from CO chondrites

Ten CAIs with diameters of several hundred μm were extracted from five different CO3 chondrites (DaG 005, DaG 025, DaG 027, DaG 083, and NWA 2187). Additionally, two CAIs from DaG 083, for which $\epsilon^{50}\text{Ti}$ data was reported in Ebert et al. (2018), were investigated for $\epsilon^{46}\text{Ti}$ and $\epsilon^{48}\text{Ti}$ isotopic compositions. In brief, most of these CO CAIs consist primarily of melilite with a rim of Mg-rich spinel and embedded spinel, perovskite, Ca-rich pyroxene (Fig. 1a), as well as minor fassaite and anorthite. Based on the categorization of refractory inclusions from the Allende meteorite (Kornacki and Wood, 1984), these CAIs from CO meteorites can therefore be considered similar to compact type A inclusions. As indicated by the occurrence of Na-rich assemblages and albite, some samples appear to have been subject to varying degrees of alteration (Fig. 1b and c).

2.2. CAIs from CM chondrite

Additionally, ten inclusions from the moderately altered CM chondrite Jbilet Winselwan (petrologic type 2.0–2.7, Bischoff et al., 2017; Friend et al., 2018) were selected for investigation of Ti isotopic compositions. These inclusions exhibit diameters of $<300\ \mu\text{m}$ (Fig. 2a and c), with the exception of CAI sample JW-6 (Fig. 2b), which exhibits a size of roughly $2400\ \mu\text{m} \times 1350\ \mu\text{m}$. More detailed information regarding the mineralogy of each sample is given in Table 2.

Of particular interest are two inclusions that differ significantly in their textural and mineralogical appearance from all other CAIs investigated here. JW-4 is an aggregate of euhedral hibonite laths with rims of calcic pyroxene and small perovskite inclusions (Fig. 3a), whereas JW-7 consists largely of spinel laths (Fig. 3b), but is similarly rimmed by calcic pyroxene and contains minor hibonite and Mg-rich spinel. Although exhibiting larger sizes compared to single PLAC and SHIB crystals, both inclusions resemble the mineralogy of such hibonite-rich inclusions, and, hence, may be related to PLACs and/or SHIBs.

3. METHODS

3.1. Sample extraction

Following petrological characterization, the CAI samples were removed from the meteorite chips using a *New*

Table 2
CAI samples from CO and CM chondrites investigated in this study.

Host meteorite	Sample	Main phases	2D-Size [μm]	TiO ₂ [wt%] ^a	total Ti after extraction [ng] ^b
<i>CO CAIs</i>					
DaG 083	DaG-1 ^c	sp, CaPx, mel, an	850 × 750	0.6	~500
	DaG-2 ^c	sp, mel, pv	900 × 720	1.0	~550
	DaG-3	mel, pv, FeNi, Na-rich alt	500 × 300	2.1	~500
DaG 005	DaG-005-1	mel, cal, sp, pv, FeNi	650 × 550	0.8	~250
DaG 025	DaG-025-1	mel, sp, fas, an	350 × 350	1.1	~85
	DaG-025-2	CaPx, sp, mel, an, neph	350 × 300	1.0	~160
DaG 027	DaG-027-1	mel, sp, pv, FeNi	650 × 550	1.7	~700
	DaG-027-2	mel, sp, hib, pv, FeNi	1000 × 600	1.5	~550
	DaG-027-3	mel, sp, CaPx, FeNi	700 × 700	1.4	~700
NWA 2187	NWA-2187-1	CaPx, an, ol, alt, FeS, FeNi	750 × 450	0.5	~150
	NWA-2187-2	alt, Fe-sp, il, Capx, FeS	700 × 550	1.1	~150
	NWA-2187-3	CaPx, FeSp, alt, pv, ol, FeS	400 × 400	1.8	~220
<i>CM CAIs</i>					
Jbilet Winselwan	JW-1	cal, sp, hib, pv	400 × 300	2.4	~200
	JW-2	sp, CaPx, ol, FeNi	200 × 300	0.5	~20
	JW-3	CaPx, sp, alt	300 × 150	2.0	~50
	JW-4	hib, CaPx, sp, pv, FeNi, alt	300 × 250	1.7	~150
	JW-5	CaPx, sp, pv, alt	400 × 500	1.5	~220
	JW-6	CaPx, sp, cal, pv	2400 × 1350	1.4	~1600
	JW-7	sp, hib, CaPx, pv	400 × 200	1.8	~75
	JW-8	ol, CaPx, sp, alt	300 × 400	0.7	~50
	JW-9	CaPx, sp, pv, alt	300 × 250	1.3	~40
	JW-10	CaPx, sp, ol, px, alt	400 × 250	0.5	~50

^a TiO₂ concentration measured prior to extraction using a JEOL 6610-LV SEM. See EA for full chemical compositions of all samples.

^b total Ti content measured after extraction using quadrupole ICPMS.

^c CAI samples from Ebert et al. (2018).

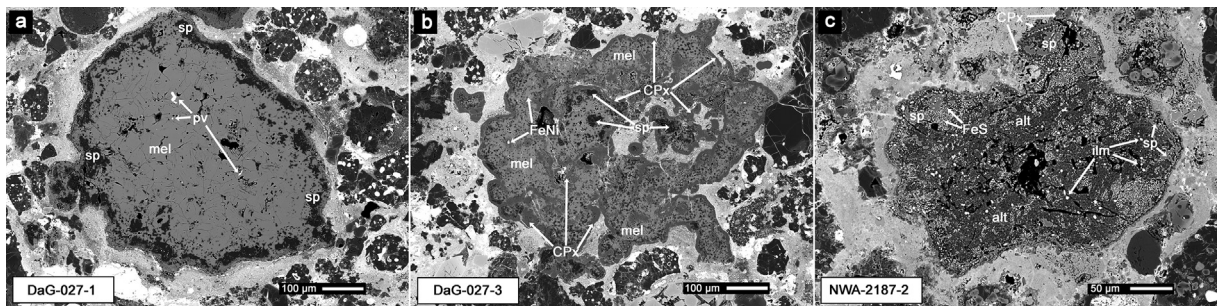


Fig. 1. Typical appearances of refractory inclusions from CO chondritic meteorites as exemplified by three CAI samples, displaying increased degrees of alteration from left to right (mel: melilite, sp: spinel, pv: perovskite, CPx: Ca-rich pyroxene, alt: alteration, ilm: ilmenite).

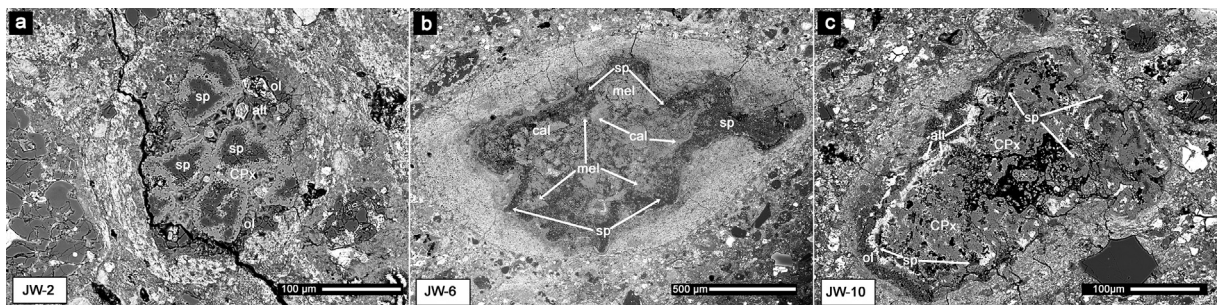


Fig. 2. Appearances of refractory inclusions from the CM chondritic meteorite Jbilet Winselwan as exemplified by three CAI samples (ol: olivine, cal: calcite).

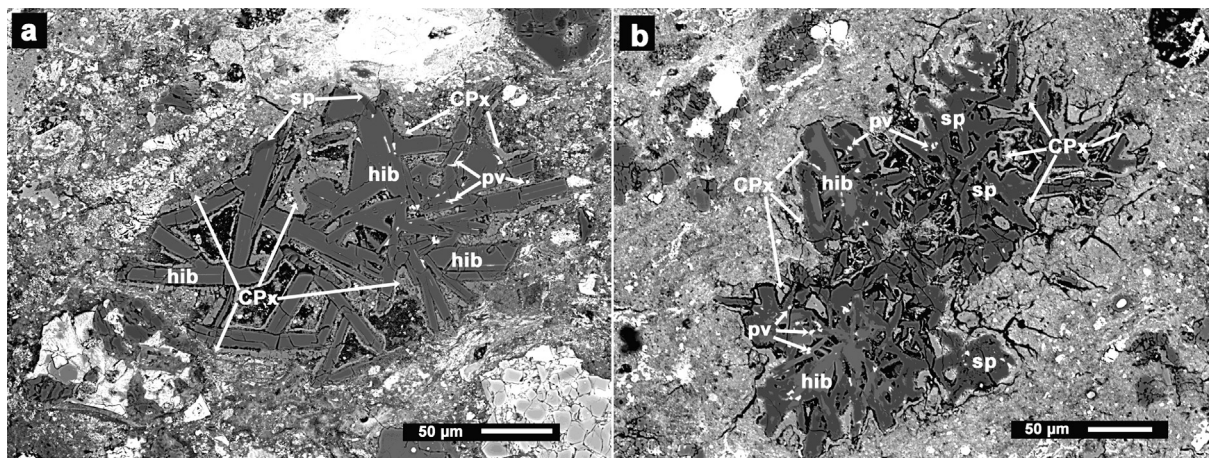


Fig. 3. SEM images of the two hibonite-rich inclusions JW-4 and JW-7. (a) JW-4 is an almost pure aggregate of hibonite laths, whereas (b) JW-7 consists of inter-grown spinel (sp) and hibonite (hib).

Wave Research Micro Mill following the method of Charlier et al. (2006). Briefly, a droplet of Milli-Q water was placed on the area of interest of the meteorite surface, being spatially confined by a piece of Parafilm with a hole in its center. Subsequently, a diamond-coated drill bit penetrated the water droplet, which captured the sample powder from the drilling process in the meteorite below. The resulting suspension was then collected with a pipette and transferred into a Savillex® PFA beaker for digestion and further chemical purification. Depending on the drill bit size and the configurations during the drilling procedure, the hemispherical drill holes were a few hundred μm in diameter, similar to the dimensions of the CAIs selected for this study. SEM images of CAIs before and after the drilling process are located in the EA (A1).

Due to the small sample sizes and the procedure used, it was not possible to accurately weigh the samples. Based on the amount of Ti available for isotope measurements and the TiO_2 content of each CAI (Table 2), it is estimated that between 10–100 μg of material was extracted per sample. Dissolving ensued via table-top digestion in concentrated HNO_3 -HF, followed by reverse aqua regia for several days on the hotplate each. After digestion, all samples were dried down and reconstituted in 12 M HNO_3 in preparation for Ti separation.

3.2. Titanium purification and evaluation of Ti blanks

As in our previous Ti isotope studies (Gerber et al., 2017; Ebert et al., 2018), purification of Ti followed the method of Zhang et al. (2011), employing a two-stage ion-exchange chromatography with pre-cleaned TODGA and Bio-Rad® AG1-X8 (200 to 400 mesh) resins. Following this procedure, the final Ti cuts were dried and treated with 20 μL H_2O_2 to remove any organic material from the resins, before being re-dissolved in 0.3 M HNO_3 -0.0015 M HF for MC-ICPMS measurements. This chemical separation procedure typically results in yields >95% (Zhang et al., 2011; Gerber et al., 2017). A more detailed description of

the chemical purification procedure used in our study is located in the EA (A2).

A procedural blank that was processed along with the CAI samples contained 2 ng Ti, which is in good agreement with blanks from previous Ti studies following the same chemistry (Zhang et al., 2011; Gerber et al., 2017). However, additional Ti may have been added during the sample removal (*i.e.*, from incidental inclusion of surrounding bulk chondrite material adjacent to the CAI samples during the drilling procedure) and needs to be accounted for (see EA A4.2). In order to quantify the amount of non-CAI Ti that was added to each individual sample, and that could have possibly diluted the anomalies towards the nucleosynthetic Ti isotope composition of the surrounding host meteorite, we applied the same correction procedure as Ebert et al. (2018):

$$\epsilon^i \text{Ti}_{\text{corr.}} = \frac{(f_{\text{CAI}}[\text{Ti}]_{\text{CAI}} + (1 - f_{\text{CAI}})[\text{Ti}]_{\text{host}})\epsilon^i \text{Ti}_{\text{meas.}} - (1 - f_{\text{CAI}})[\text{Ti}]_{\text{host}}\epsilon^i \text{Ti}_{\text{host}}}{f_{\text{CAI}}[\text{Ti}]_{\text{CAI}}}$$

In this equation, f_{CAI} denotes the fraction of CAI material, which was quantified by point counting technique for each sample. Further, $[\text{Ti}]_i$ is the Ti concentration in the CAIs (Table 2) and the chondritic host meteorites (≈ 0.06 wt% Ti, Friedrich et al., 2002; Braukmüller et al., 2018; Friend et al., 2018), respectively. The resulting corrections are largest in $\epsilon^{50}\text{Ti}$, ranging from 0.04 (CAIs NWA-2187-1 and JW-1) up to 1.12 (CAI JW-2). Uncertainties on these corrections are propagated assuming a 50% uncertainty to the final isotopic compositions. In the following sections, the given Ti isotopic compositions of CAIs always refer to the corrected values (the uncorrected Ti isotopic compositions can be found in the EA A4.2).

3.3. Ti isotopic measurements

Titanium isotope measurements were performed as outlined in Ebert et al. (2018), using the Neptune Plus MC-ICPMS in combination with a Cetac Aridus II® desolvator at the Institut für Planetologie in Münster and internally

normalizing to $^{49}\text{Ti}/^{47}\text{Ti} = 0.749766$. However, in addition to $\epsilon^{50}\text{Ti}$ data, we also report anomalies for the isotopes $\epsilon^{46}\text{Ti}$ and $\epsilon^{48}\text{Ti}$, which we analyzed as outlined in Gerber et al. (2017). All Ti isotope data reduction was manually performed off-line and interfering element isotope ratios ($^{46}\text{Ca}/^{44}\text{Ca}$, $^{48}\text{Ca}/^{44}\text{Ca}$, $^{50}\text{V}/^{51}\text{V}$, and $^{50}\text{Cr}/^{53}\text{Cr}$) were manually adjusted from doped standard solution tests (Zhang et al., 2011). Pre-dilutions of all samples were checked prior to isotope measurements to ensure that interfering elements were below the maximum thresholds determined by Zhang et al. (2011). Results are given in the ϵ -notation, as the deviation in parts per ten thousand relative to the Origins Lab OL-Ti standard:

$$\epsilon^i\text{Ti} = \left[\frac{\left(\frac{{}^i\text{Ti}/{}^{47}\text{Ti}}{\text{sample}} \right)}{\left(\frac{{}^i\text{Ti}/{}^{47}\text{Ti}}{\text{standard}} \right)} - 1 \right] \times 10,000.$$

The sub- ϵ analytical uncertainty for all three Ti isotopes achieved here (Table 3) represents a roughly 100-fold improvement in precision compared to *in-situ* techniques, such as SIMS, with which similarly-sized samples previously had to be investigated (e.g., Ireland, 1990; Liu et al., 2009; Kööp et al., 2016a; 2016b; 2018a). More details regarding the instrumental setup and operating conditions of our Ti isotope measurements are presented in the EA (A3).

4. RESULTS

Sample means and associated uncertainties are shown in Table 3 and Figs. 4–6.

Both terrestrial standards BCR-2 and BHVO-2 yield $\epsilon^i\text{Ti}$ values indistinguishable from those previously reported for these samples (e.g., Zhang et al., 2011; Gerber et al., 2017), demonstrating the accuracy of our method. Additionally, the CV CAI *Egg-2 high* exhibits a Ti isotopic composition typical for CAIs from CV chondrites (e.g., Trinquier et al., 2009: $\epsilon^{50}\text{Ti}_{\text{CAI}} \approx 9$) and is in agreement with previously published Ti isotopic composition for this sample (Ebert et al., 2018).

All twelve CAIs from CO chondrites investigated here show resolved excesses in $\epsilon^{50}\text{Ti}$ relative to terrestrial isotope abundances, ranging from 2.9 to 9.3 (Table 3). Anomalies in $\epsilon^{46}\text{Ti}$ range from 0.1 to 2.0, with ten out of twelve CO CAIs resolved from terrestrial isotope compositions. Similarly, all eight regular (i.e., excluding samples JW-4 and JW-7) CAIs from the CM2 chondrite Jbilet Winselwan exhibit positive isotope anomalies in $\epsilon^{50}\text{Ti}$ and seven out of eight show resolved excesses in $\epsilon^{46}\text{Ti}$ (Fig. 4). Although some scatter is present, most of the CAI samples analyzed here fall along the correlation line of $\epsilon^{46}\text{Ti} = (0.162 \pm 0.030) \times \epsilon^{50}\text{Ti} + (0.15 \pm 0.27)$ as defined by an array of 49 CAIs from the Allende meteorite (Davis et al., 2018). To our knowledge, CAI sample JW-6 has the lowest $\epsilon^{50}\text{Ti}$ value ever reported for any regular CAI and appears to be the first such sample with a resolved deficit in $\epsilon^{46}\text{Ti}$ (Fig. 4).

In contrast, the two exceptional inclusions JW-4 (consisting largely of hibonite) and JW-7 (consisting primarily

of spinel) show highly anomalous Ti isotopic compositions (Table 3). They appear to be the only samples of this study showing large anomalies in $\epsilon^{48}\text{Ti}$, where most CAIs show no or barely resolved isotope anomalies (Leya et al., 2009; Trinquier et al., 2009; Davis et al., 2018; this study). Both inclusions plot far away from the correlations defined by Allende CAIs (Fig. 5) and exhibit distinct isotope patterns in ${}^i\text{Ti}$ vs. $\epsilon^i\text{Ti}$ space (Fig. 6).

5. DISCUSSION

5.1. Origin of Ti isotope variability in CAIs

The CAIs from CO and CM chondrites investigated in this study show significant Ti isotope variability from one sample to another. Similar variability in nucleosynthetic isotope compositions has been previously observed for larger CV CAIs in both Ti (e.g., Williams et al., 2016; Davis et al., 2018), as well as in other elements, e.g., Mo (Burkhardt et al., 2011), W (Kruijjer et al., 2014), Ni (Render et al., 2018), and Sr (Myojo et al., 2018). These previous studies have ascribed such isotope variability for CAIs primarily to the heterogeneous distribution of one or multiple anomalous carrier phases within the CAI-forming region.

However, such interpretations are critical to the nucleosynthetic signatures of samples being primary signals. Although Ti is an immobile and refractory element, it is noteworthy that the CAIs investigated here are significantly smaller compared to the CV CAIs that were investigated in the above-mentioned studies (i.e., sub-mm sized vs. cm-sized) and, in addition, are partially derived from desert meteorite finds. Due to their terrestrial residence time and higher surface-area-to-volume-ratios, the specific CAIs investigated here are potentially more susceptible to possible contamination with non-indigenous Ti. Such addition of foreign Ti into the measured CAI-samples could theoretically have occurred (1) during (hydro-)thermal metamorphism on their respective parent bodies, (2) from desert weathering during their terrestrial residence time, or (3) by incidental inclusion of host meteorite material during the drilling process (see Section 3.2). Each of these three possibilities would lead to variable dilution of the original Ti isotope anomalies of the CAIs, either towards terrestrial Ti isotope compositions (i.e., $\epsilon^i\text{Ti} \equiv 0$) or towards the Ti isotopic compositions of their bulk host meteorites (i.e., $\epsilon^{46}\text{Ti} \approx 0.5$, $\epsilon^{48}\text{Ti} \approx 0$, $\epsilon^{50}\text{Ti} \approx 3$, Trinquier et al., 2009). These possibilities are addressed at length in the EA. In brief, we do not see evidence of significant consequences on the Ti isotopic compositions from alteration processes, most likely due to the immobile character of Ti. Although the possibility of slight effects from minor, non-indigenous Ti contributions cannot be entirely excluded, we show that the vast majority of isotope variability in this particular set of CAIs is inherent to these samples. Together with similar observations from previous studies (e.g., Davis et al., 2018; Ebert et al., 2018), this indicates that heterogeneity of Ti isotopes is a feature of CAIs as a group, regardless of host meteorite and likely reflects a primordial Ti isotope heterogeneity of their formation region.

Table 3
Mass-independent Ti isotopic compositions of terrestrial and CAI samples.

Type/host meteorite	Sample	f_{CAI}	N^{a}	ppb Ti_{sol}	$\epsilon^{46}\text{Ti}^{\text{b}}$	$\epsilon^{48}\text{Ti}^{\text{b}}$	$\epsilon^{50}\text{Ti}^{\text{b}}$
Allende (CV3)	Egg-2 high	–	4	100	2.24 ± 0.18	0.81 ± 0.68	9.73 ± 0.13
Terrestrial basalt standard	BCR-2	–	15	100	-0.09 ± 0.12	-0.02 ± 0.08	-0.04 ± 0.07
			7	50	0.07 ± 0.17	0.04 ± 0.21	-0.05 ± 0.25
Terrestrial basalt standard	BHVO-2	–	14	100	0.02 ± 0.11	-0.07 ± 0.09	-0.08 ± 0.10
			9	50	-0.11 ± 0.25	-0.37 ± 0.17	-0.03 ± 0.17
Basalt average			45		-0.04 ± 0.07	-0.06 ± 0.06	-0.06 ± 0.05
External reproducibility				100	± 0.43	± 0.31	± 0.31
				50	± 0.60	± 0.47	± 0.59
<i>CO CAIs</i>							
DaG 083	DaG-1 ^c	1.00	5	100	1.33 ± 0.39	0.00 ± 0.16	8.93 ± 0.28
	DaG-2 ^c	1.00	5	100	1.64 ± 0.24	0.11 ± 0.32	9.31 ± 0.07
	DaG-3	0.80	5	100	2.00 ± 0.28	-0.08 ± 0.33	7.63 ± 0.22
DaG 005	DaG-005-1	0.90	5	100	1.77 ± 0.16	0.82 ± 0.44	6.89 ± 0.21
DaG 025	DaG-025-1 ^d	0.63	2	50	1.43 ± 0.60	–	6.03 ± 0.61
	DaG-025-2	0.44	2	100	1.87 ± 0.43	0.70 ± 0.31	9.32 ± 0.44
DaG 027	DaG-027-1	1.00	5	100	0.06 ± 0.35	0.06 ± 0.10	2.91 ± 0.11
	DaG-027-2	1.00	5	100	1.84 ± 0.29	0.79 ± 0.15	6.78 ± 0.05
	DaG-027-3 ^d	1.00	5	100	0.75 ± 0.32	–	4.72 ± 0.27
NWA 2187	NWA-2187-1	0.95	2	100	1.46 ± 0.43	0.57 ± 0.31	7.92 ± 0.31
	NWA-2187-2	0.32	2	100	1.15 ± 0.43	-0.01 ± 0.31	5.55 ± 0.42
	NWA-2187-3 ^d	0.61	5	100	0.17 ± 0.36	–	2.97 ± 0.38
<i>CM CAIs</i>							
Jbilet Winselwahn	JW-1	0.76	5	100	0.91 ± 0.14	0.02 ± 0.06	5.61 ± 0.36
	JW-2 ^d	0.52	1	35	–	–	6.15 ± 1.05
	JW-3	0.22	2	50	1.38 ± 0.60	-0.46 ± 0.47	6.16 ± 0.71
	JW-5	0.54	4	100	1.74 ± 0.14	0.41 ± 0.09	8.40 ± 0.18
	JW-6	1.00	10	100	-0.28 ± 0.15	0.37 ± 0.06	1.43 ± 0.13
	JW-8	0.74	2	50	1.67 ± 0.60	0.74 ± 0.47	6.10 ± 0.63
	JW-9	0.78	2	50	0.90 ± 0.60	-0.81 ± 0.47	5.43 ± 0.66
	JW-10	0.70	2	50	1.18 ± 0.60	-0.03 ± 0.47	6.40 ± 0.62
	JW-4 (hibonite-rich)	0.37	3	100	-6.65 ± 0.44	12.91 ± 0.36	-18.44 ± 0.42
	JW-7 (spinel-rich)	0.82	2	75	-3.07 ± 0.52	-11.70 ± 0.45	14.41 ± 0.52

^a Number of analyses of the same sample solution.

^b Nucleosynthetic Ti isotope data are reported using the ϵ -notation relative to the OL-Ti reference standard and are mass-bias corrected by internally normalizing to $^{49}\text{Ti}/^{47}\text{Ti} = 0.749766$ and using the exponential law. For samples measured > 3 times, uncertainties are twofold standard errors (2 s.e.) from replicate analyses; for samples measured ≤ 3 times, uncertainties reflect the external reproducibility as defined by $2 \times$ standard deviation (2 s.d.) of repeated analyses of BCR-2 and BHVO-2. Titanium isotope anomalies are corrected for slight contributions of non-indigenous Ti where necessary (see Section 3.2 and EA A4.2), with f_{CAI} denoting the fraction of CAI material per sample.

^c ^{50}Ti isotope data from Ebert et al. (2018).

^d Ti isotopic compositions only partially reported due to low total Ti contents and interferences from ^{46}Ca and/or ^{48}Ca during these measurements.

One important consequence of this Ti isotope variability is that the correlated isotope anomalies in $\epsilon^{46}\text{Ti}$ and $\epsilon^{50}\text{Ti}$ can be used as another tool for comparing the provenance of samples. This $\epsilon^{46}\text{Ti}$ - $\epsilon^{50}\text{Ti}$ -correlation, which was previously noted for Allende CAIs (Davis et al., 2018) and for bulk Solar System materials (e.g., Trinquier et al., 2009; Zhang et al., 2011), is now also shown to be present in CAIs from both CO and CM chondrites. Such combined excesses in a neutron-poor (^{46}Ti) and a neutron-rich (^{50}Ti) isotope are particularly interesting because the two isotopes are expected to have distinct nucleosynthetic origins (i.e., they formed in distinct stellar environments). Whereas ^{46}Ti is related to Type II supernovae, ^{50}Ti is thought to derive from either Type Ia or electron-capture supernovae

(e.g., Wanajo et al., 2013). The fact that excesses in both isotopes are correlated in the Solar System materials has been ascribed to thermal processing of multiple presolar phases (e.g., Trinquier et al., 2009). However, it is currently unknown whether the Ti isotopic signatures in CAIs reflect the same anomalous carrier phase(s) as in bulk meteorites.

For instance, Dauphas et al. (2014) speculated that variable amounts of perovskite could explain correlated anomalies in $\epsilon^{48}\text{Ca}$ and $\epsilon^{50}\text{Ti}$ in bulk meteorites and CAIs. Perovskite is a highly refractory mineral that is present in most CAIs and contains the right stoichiometry (CaTiO_3 , i.e., $\text{Ca}:\text{Ti} = 1$) to account for the slope ($m = 1.09 \pm 0.11$) of correlated anomalies in both elements (Dauphas et al., 2014). However, no correlation between perovskite content

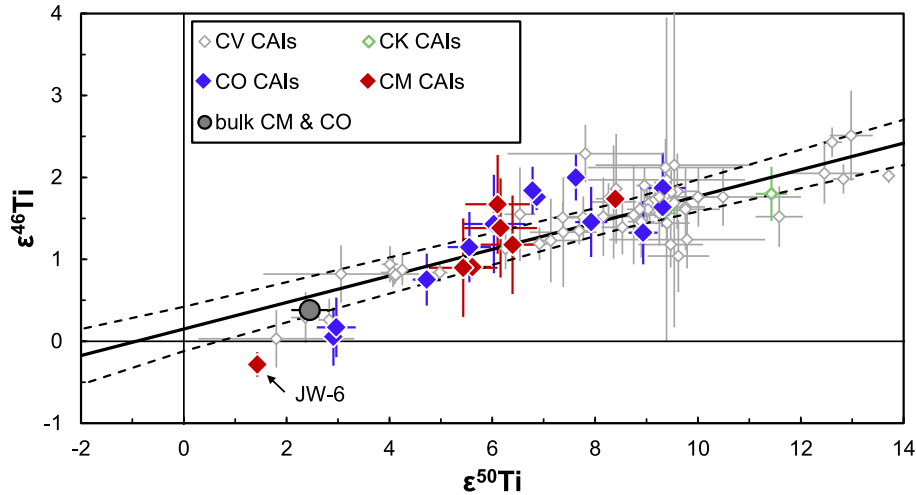


Fig. 4. Nucleosynthetic Ti isotopic compositions of CAIs from CO and CM chondritic meteorites reported here, along with literature data for 59 CAIs from CV chondrites (Leya et al., 2009; Trinquier et al., 2009; Davis et al., 2018), two CAIs from CK chondrites (Torrano et al., 2017), and of bulk CM and CO meteorites (Trinquier et al., 2009) for comparison. The solid black line and related dashed error envelopes represent a best-fit regression for 49 Allende CAIs, taken from Davis et al. (2018).

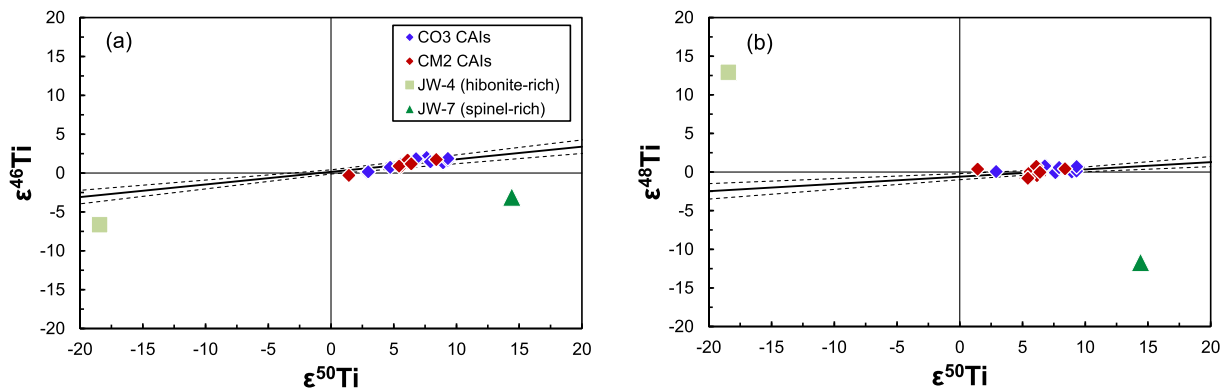


Fig. 5. (a) An expanded version of Fig. 4 showing Ti isotopic compositions of hibonite-rich samples JW-4 and JW-7 in relation to the regular CAIs investigated here and including the regression from Davis et al. (2018), (b) Same plot, but with $\epsilon^{48}\text{Ti}$ vs. $\epsilon^{50}\text{Ti}$. Uncertainties are smaller than the symbols in both plots.

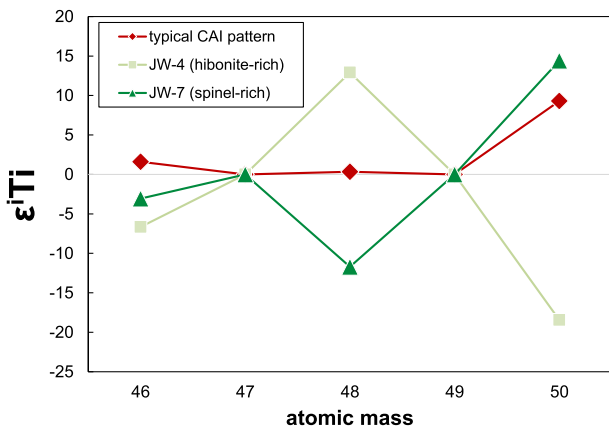


Fig. 6. Titanium isotope anomalies for JW-4 and JW-7 (uncertainties are smaller than the symbols) compared to a Ti isotope signature typical for CAIs (Trinquier et al., 2009; Davis et al., 2018; this study).

and the overall magnitude in Ti isotope anomalies was observed in the samples investigated here. Nevertheless, the modal proportion of perovskite in a given CAI does not necessarily correspond to the fraction of perovskite present in the CAI precursor material, the composition of which was likely modified during thermal processing in the high-temperature formation regime of CAIs.

Alternatively, as one of the most abundant and best-studied presolar carriers, silicon carbide (SiC) is another candidate phase, possibly responsible for isotope anomalies in Ti (and other elements). The stellar origin of SiC is generally accepted to be located in the envelope of AGB stars, in which the *s*-process of nucleosynthesis is thought to take place. The effects of the *s*-process of nucleosynthesis on elements of the Fe-peak (*i.e.*, Ca, Ti, Cr, Ni, Fe, Zn) were recently modeled by Wasserburg et al. (2015). These authors found that the *s*-process leads to enrichments of ^{46}Ti , ^{47}Ti , ^{49}Ti , and ^{50}Ti when normalized to a constant ^{48}Ti abundance. This prediction is in good agreement with

analyses of mainstream SiC data (e.g., Amari et al., 2001; Gyngard et al., 2018) (Fig. 7a). For better comparison with the CAI isotope data, it is necessary to internally normalize the presolar grain and model data. Interestingly, even after such internal normalization to a fixed $^{47}\text{Ti}/^{49}\text{Ti}$, excesses in $\epsilon^{46}\text{Ti}$ and $\epsilon^{50}\text{Ti}$ are preserved (Fig. 7b), indicating that matter processed through the *s*-process could indeed, at least theoretically, explain such correlated anomalies in neutron-poor (^{46}Ti) and neutron-rich (^{50}Ti) isotopes.

At the same time, however, the *s*-process leads to significant depletions in $\epsilon^{48}\text{Ti}$, which are not observed either in CAIs or in bulk meteorite isotope data. Additionally, the ratio of anomalies in $\epsilon^{46}\text{Ti}$ and $\epsilon^{50}\text{Ti}$ is different from those observed in CAIs or bulk Solar System materials (Fig. 7b). Therefore, if mainstream SiC were a main contributor to the Ti isotope signatures of extraterrestrial materials, at least one more component, enriched in ^{48}Ti and ^{50}Ti , would be required to explain the full Ti isotopic compositions that are reported for CAIs. As such, a mix of multiple presolar phases is needed to reproduce the isotopic fingerprint of the CAI forming region, reflecting the contribution of isotopically distinct matter from multiple nucleosynthetic sources, (e.g., Shollenberger et al., 2018b). One of these isotopically anomalous carrier phases could resemble, or even be represented by hibonite-rich PLAC grains, which have been shown to be highly anomalous in $\epsilon^{50}\text{Ti}$, while their $\epsilon^{46}\text{Ti}$ or $\epsilon^{48}\text{Ti}$ isotopic compositions are not resolved from terrestrial abundances (e.g., Kööp et al., 2016a).

5.2. Isotopic similarity between regular CAIs from different chondrite groups

Despite the heterogeneous distribution of presolar matter, which causes the variable nucleosynthetic Ti isotope anomalies in CAIs from CO and CM chondrites, there remains evidence for a close genetic relationship between these two populations. Not only do CAIs from both of

these chondrite groups show indistinguishable ranges of nucleosynthetic isotope anomalies in all three Ti isotopes, but they also plot on or very close to a single $\epsilon^{46}\text{Ti}$ - $\epsilon^{50}\text{Ti}$ correlation line. Taken together, the isotope data suggest that CAIs from CO and CM meteorites sampled a similar mixture of presolar matter and, thus, support a shared genetic heritage. Intriguingly, these Ti isotopic similarities are not only found among CO and CM CAIs, but also with regards to CV and CK CAIs:

Previous studies using high-precision mass spectrometry have reported very similar ranges in the Ti isotope signatures of CAIs from Allende and other CV chondrites (e.g., Niederer et al., 1981; Niemeyer and Lugmair, 1981; Leya et al., 2009; Trinquier et al., 2009; Davis et al., 2018). In addition, $\epsilon^{50}\text{Ti}$ isotope data exists for CV CAIs that were analyzed by laser ablation (LA-)ICPMS (Williams et al., 2016; Jordan et al., 2017; Simon et al., 2017). Whereas most CAIs analyzed in these studies are in good agreement with the range in $\epsilon^{50}\text{Ti}$ obtained in high-precision mass spectrometry studies, Simon et al. (2017) report nucleosynthetic excesses in $\epsilon^{50}\text{Ti}$ of ~ 40 in one fine-grained Allende CAI ('461B'). This sample also stands out by containing significant amounts of hibonite and an extraordinarily high Cr/Ti ratio of ~ 7.5 . However, even if the applied Cr-stripping correction is working for this high Cr sample, this CAI appears to be an exceptional sample, chemically, mineralogically, and isotopically, and is conceivably not representative of the CAI-forming region in whole.

To this point, only two CAIs from meteorites of the CK carbonaceous chondrite group have been analyzed for Ti isotopes (Torranó et al., 2017), but these also exhibit Ti isotope anomalies indistinguishable to those of CV CAIs. More importantly, essentially all of these CAIs investigated so far—regardless of type, REE pattern, or host meteorite—appear to be consistent with the $\epsilon^{46}\text{Ti}$ - $\epsilon^{50}\text{Ti}$ correlation line reported by Davis et al. (2018). On face value,

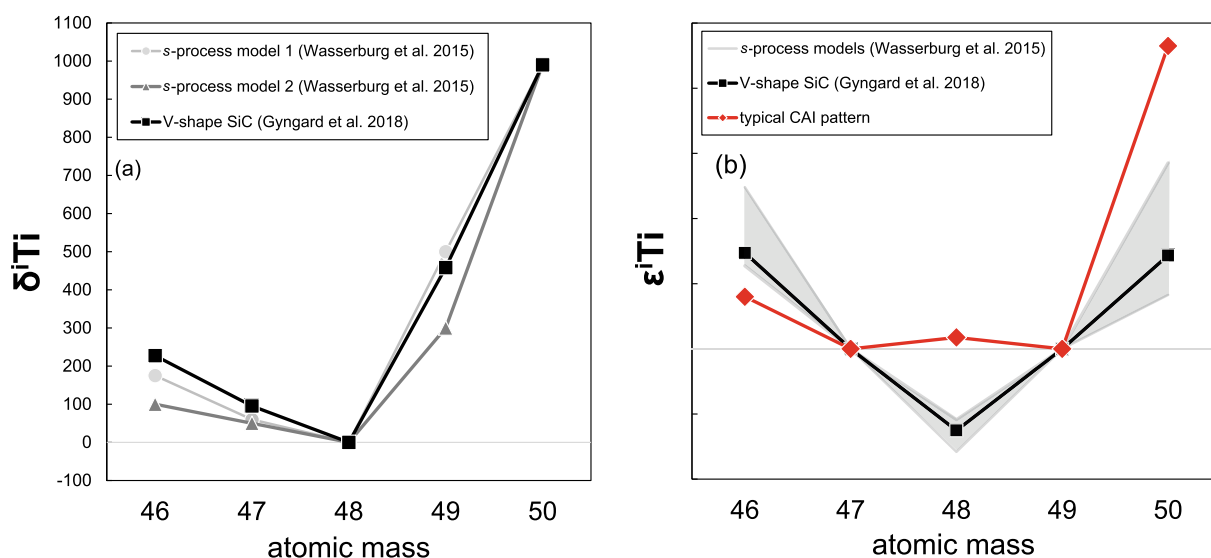


Fig. 7. (a) Modeled effects of the *s*-process of nucleosynthesis in Ti isotopes (Wasserburg et al., 2015) compared to data for V-shape SiC from Gyngard et al. (2018) relative to a fixed ^{48}Ti and ^{50}Ti , (b) renormalization to a fixed ^{47}Ti - ^{49}Ti ratio together with the pattern of a typical CAI [anomalies not to scale].

these combined studies therefore indicate that CAIs from CO, CM, CK, and CV meteorites are genetically related and most likely derived from a single common reservoir, but vary only slightly from incorporation of a (or multiple) Ti carrier(s). In addition, six CAIs from ordinary chondrites yielded similar ^{50}Ti excesses (Ebert et al., 2018), indicating they were formed in a single common formation region together with CAIs from CV, CO, CM, and CK chondrites.

One sample, JW-6, stands out by showing the least anomalous Ti isotopic compositions, both with regards to samples from this study (Table 3) and from the literature (Fig. 4). Furthermore, this specific sample is clearly resolved from the best-fit correlation line defined by the array of Allende CAIs from Davis et al. (2018). The reason for this is currently not fully understood, but the most likely explanation for scatter around the $\varepsilon^{46}\text{Ti}$ - $\varepsilon^{50}\text{Ti}$ correlation (MSWD of 3.7 reported by Davis et al. (2018)) is that the range of Ti isotopic compositions in CAIs does not reflect a simple two-component mixture. For example, carbonaceous meteorites of the CM group have been shown to contain the highest abundances of primitive and highly unequilibrated matter, including presolar grains and hibonite-rich inclusions (e.g., Kööp et al., 2016b). Assimilation or incorporation of such grains or components with isotopically highly anomalous Ti into CAI precursors could have a radical effect on one isotope, while not (or disparately) impacting the other Ti isotopes, significantly altering its captured isotopic signature. It is additionally noteworthy that JW-6 also stands out with an unusual mineralogy for CAIs, containing significant amounts of calcite (CaCO_3) (Fig. 2b), suggesting that it could have been subject to a rather uncommon history for CAIs and is thus not representative (e.g., Lee and Greenwood, 1994).

In spite of the exceptional deviation of this sample, it appears that regular CAIs from various meteorites form a population of extraterrestrial samples with indistinguishable ranges of Ti isotope anomalies. This nucleosynthetic conformity in Ti isotopes among CAIs is in good agreement with similar conclusions from previous investigations of mass-independent isotope variability in O, reporting similar ^{16}O -enrichments for regular CAIs from CO, CM, and ordinary chondrites (McKeegan et al., 1998; Wasson et al., 2001; Itoh et al., 2004; Matzel et al., 2013; Jacobsen et al., 2014; Ushikubo et al., 2017). Additionally, the inferred $(^{26}\text{Al}/^{27}\text{Al})_0$ of CAIs from CO ($5.05 \pm 0.18 \times 10^{-5}$), CM ($4.88 \pm 0.48 \times 10^{-5}$) and ordinary chondrites ($\sim 5 \times 10^{-5}$) (Russell et al., 1996; Matzel et al., 2013; Ushikubo et al., 2017) exhibit (near-)canonical values established using large CAIs from CV meteorites (i.e., 5.23×10^{-5} , Jacobsen et al., 2008). Assuming that ^{26}Al was homogeneously distributed throughout the solar nebula (or at least in the CAI formation region), this indicates that inclusions from CO and CM meteorites, together with CV and CK CAIs likely formed in a short timeframe. In summary, these data suggest that regular CAIs (i.e., excluding FUN CAIs and hibonite-rich objects) from different chondrite groups formed at about the same time, in the same location, and from similar matter. The single reservoir from which these CAIs were formed appears to have been

enriched in ^{16}O , ^{46}Ti , ^{50}Ti , and several others relative to terrestrial isotope abundances.

Since these various chondrite groups are thought to represent accretion regions at different distances from the Sun (e.g., Wood, 2005; Warren, 2011; Render et al., 2017; Desch et al., 2018), our data demonstrate that large-scale transport of CAIs over a significant range of heliocentric distances must have occurred before the CV, CK, CO, and CM parent bodies accreted in their respective orbits. Intriguingly, a few micrometer-sized CAI-like particles have been found in samples of the comet 81P/Wild 2, which is thought to have formed >10 AU (Brownlee et al., 2006). In detail, the mineralogical composition and the ^{16}O -rich nature of the CAI-like particle *Inti* (McKeegan et al., 2006; Simon et al., 2008) bears resemblance to CAIs, however, another refractory fragment termed *Coki* has an initial $^{26}\text{Al}/^{27}\text{Al}$ of $\leq 1 \times 10^{-5}$ (Matzel et al., 2010), significantly less than the canonical CAI value (Jacobsen et al., 2008). As no nucleosynthetic isotope data are available for these samples, it is currently unknown whether the refractory particles found in 81P/Wild 2 indeed represent fragments of regular CAIs or of other isotopically unrelated material. However, the here demonstrated presence of regular refractory inclusions in distally formed CM chondrites is consistent with highly refractory materials found in comets that are thought to have formed beyond the ice line (Brownlee et al., 2006).

In summary, the broad distribution of refractory matter sharing nucleosynthetic signatures in a variety of outer Solar System materials mandates their formation in a single high-temperature environment paired with efficient transport over large distances. The exact nature of the processes involved in transporting CAIs is yet unknown, however, multiple mechanisms, such as meridional flows (Ciesla, 2010) or viscous spreading (e.g., Yang and Ciesla, 2012) have been proposed. The distinct size populations of CAIs in CV/CK/CO/CM chondrites and comets may provide clues to the transport mechanisms responsible for distributing refractory inclusions into different outer Solar System regions.

5.3. The two exceptional inclusions JW-4 and JW-7

Two refractory inclusions from Jbilet Winselwan, JW-4 and JW-7, exhibit different textural and mineralogical appearances compared to other CAIs, possibly hinting at a different formation history and/or genetic heritage. These samples also exhibit highly anomalous and seemingly unrelated Ti isotopic compositions (Table 2, Fig. 6), and as such, they are treated separately in this section.

Petrographically, JW-4 consists of euhedrally shaped lath-shaped crystals of hibonite, whereas JW-7 is primarily made up of spinel laths, respectively (Fig. 3a and b), indicating these inclusions formed by idiomorphic crystallization from a gas phase in the solar nebula. Ca-rich pyroxene fills out interstices in both inclusions and surrounds the aggregates with an outward rim, possibly indicating the continued condensation sequence from a gas of solar composition after further cooling. However, although these mineralogical resemblances with regards to single

PLAC and SHIB crystals exist, a genetic relationship can at this point neither be denied nor confirmed.

In terms of Ti isotopic compositions, both JW-4 and JW-7 exhibit deficits in $\epsilon^{46}\text{Ti}$, whereas their $\epsilon^{50}\text{Ti}$ anomalies are negative (JW-4) and positive (JW-7), respectively. Additionally, these two inclusions show large isotope anomalies in $\epsilon^{48}\text{Ti}$ (Figs. 5–6), whereas regular CAIs show no or only very limited $\epsilon^{48}\text{Ti}$ anomalies (Davis et al., 2018; this study). The reason for these excesses in $\epsilon^{48}\text{Ti}$ is not yet fully understood, however, we note that the overall Ti isotopic compositions of JW-4 and JW-7 cannot be explained by variability in the normalizing isotope pair ^{47}Ti or ^{49}Ti , either (see EA A6). Instead, the nucleosynthetic signatures of these inclusions must result from anomalous abundances in multiple Ti isotopes relative to terrestrial values.

Due to their related mineralogy and exceptional isotopic signatures, it is tempting to compare the Ti isotopic compositions of the two hibonite-rich aggregates studied here with Ti isotope data for single PLAC and SHIB crystals that have been previously analyzed using *in-situ* techniques (e.g., Ireland, 1990; Liu et al., 2009; Kööp et al., 2016a; 2016b; 2018a). Unfortunately, due to the larger analytical uncertainties of SIMS measurements, it is currently not possible to resolve systematic differences or assign genetic links in the Ti isotopic compositions between single hibonite-rich crystals and the two hibonite-rich aggregates presented here (Fig. 8), nor is it possible to identify meaningful correlations from these two inclusions alone (Fig. 5). Similarly, no conclusive relationships to FUN CAIs (Kööp et al., 2018b) can be identified in Fig. 8. It can be stated at this point that both JW-4 and JW-7 exhibit exceptional mineralogical compositions and isotopic signatures that are clearly distinct from regular CAIs and appear more similar to characteristics reported for PLACs and SHIBs. Intriguingly, Ti isotopic compositions of individual PLAC samples occasionally appear to occupy similar isotopic compositions in $\epsilon^{46}\text{Ti}$ vs. $\epsilon^{50}\text{Ti}$ space (e.g., Kööp et al., 2016a), indicating these single crystal samples could be derived from hibonite-rich aggregates similar to JW-4 and JW-7. If this is true, not only PLACs but also SHIBs would lack the $\epsilon^{46}\text{Ti}$ - $\epsilon^{50}\text{Ti}$ correlation found in regular CAIs.

The differences between Ti isotopic signatures of JW-4, JW-7, and regular CAIs could be interpreted as each of

these refractory materials having been built in different regions of the protoplanetary disk. For instance, the two hibonite(-spinel)-rich aggregates could have been derived from localized domains, where genetically distinct mixtures of presolar matter were present, or alternatively, where different processes or physicochemical conditions (*i.e.*, temperature, pressure, redox conditions) were prevailing. Such disparate environmental prerequisites could render variable processing of presolar matter, for instance, causing the selective separation of evaporates and residues, corresponding to their cosmochemical properties.

Alternatively, it has been suggested that major components in the protoplanetary disk were initially isotopically heterogeneous and equilibrated to varying degrees over time. For instance, Krot et al. (2010) suggested that the primordial solar nebula gas was initially rich in ^{16}O and the primordial dust ^{16}O -poor. Enrichments or depletions in ^{16}O observed in diverse extraterrestrial materials could hence be explained by progressive changes in the prevailing regimes (*i.e.*, at different times with different conditions and/or processes being present) or by formation in portions of the protoplanetary disk with variable gas/dust ratios. Along with continuous equilibration of dust and gas in the solar nebula, mass-independent isotopic variations would thus evolve from disparate to more homogeneous values over time. Although Ti features a significantly higher condensation temperature compared to O and is thus not expected to be pervasive in the solar nebula gas at significant quantities for as long as O, a similar case can be made to explain isotopic differences between diverse refractory materials: Continuous blending and thermal processing could have progressively homogenized different heterogeneously distributed Ti-bearing carrier phases over time, resulting in decreasing ranges of isotopic compositions in subsequently formed types of refractory matter.

Although it is currently not possible to assign exact chronological positions to JW-4 and JW-7, it is thus a perhaps more likely possibility that these two inclusions derive from the same localized region in which regular CAIs formed, but reflect different points in time. In other words, these two hibonite-rich aggregates may have formed from a poorly mixed pool of gas and dust, which then evolved to a more homogenized reservoir and cooled down, allowing for condensation of regular CAIs. In a similar manner, PLACs

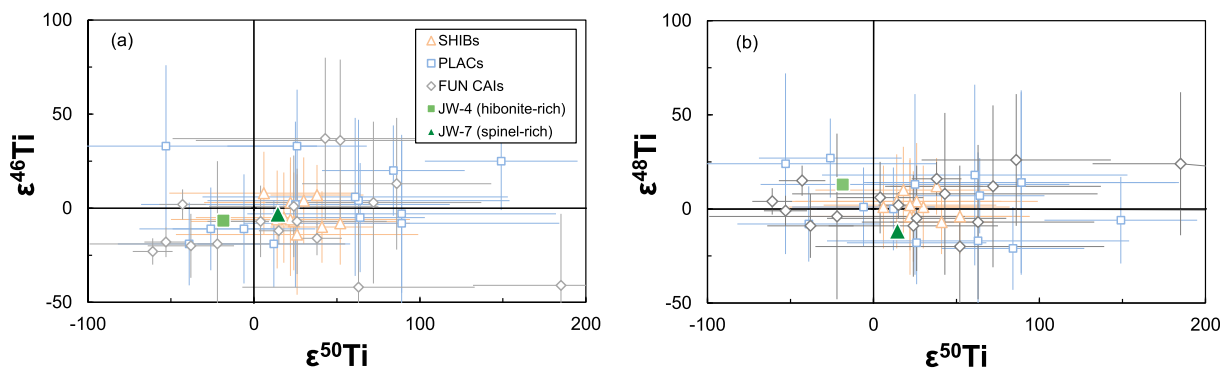


Fig. 8. Titanium isotope data for JW-4 and JW-7 compared to *in-situ* analyses of single PLAC and SHIB crystals from Kööp et al. (2016a; 2016b), as well as FUN inclusions (Park et al., 2014; Kööp et al., 2018b) [note that PLACs can be up to 10 times more anomalous than shown here].

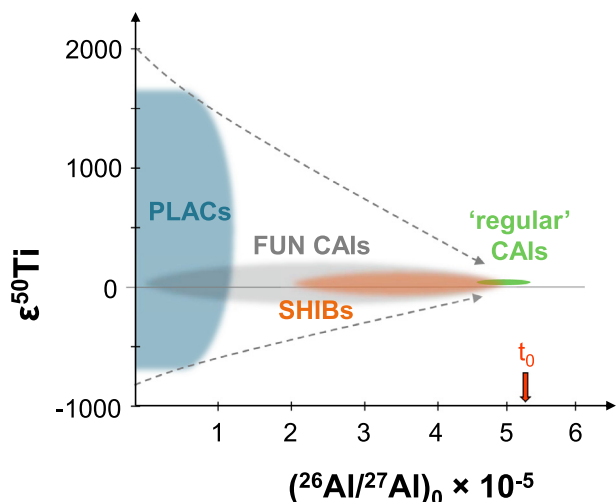


Fig. 9. Relationship between $\epsilon^{50}\text{Ti}$ and inferred initial $(^{26}\text{Al}/^{27}\text{Al})_0$ in a variety of refractory materials. Isotopically unequilibrated PLACs lack ^{26}Al , and grade towards less anomalous inclusions, approaching more homogenous regular CAIs with canonical $(^{26}\text{Al}/^{27}\text{Al})_0$, shown as t_0 (Jacobsen et al., 2008). References for Ti isotope and ^{26}Al data given in the main text.

have previously been suggested to have formed prior to regular CAIs to explain their highly unequilibrated isotopic nature, the ultra-refractory mineralogical and chemical compositions, and the lack of evidence for incorporation of ^{26}Al (Kööp et al., 2016a).

Collectively, these combined isotope studies hint at the existence of multiple generations of refractory matter throughout the early history of the Solar System, proceeding from isotopically highly unequilibrated PLACs and FUN CAIs to less anomalous SHIBs and finally to regular CAIs before bulk meteorites started accreting (Fig. 9). In this case, statistically significant sets of each generation of refractory matter (i.e. hibonite-rich grains, FUN inclusions, and regular CAIs) should yield average Ti isotopic composition close to that of regular CAIs (i.e., $\epsilon^{46}\text{Ti} \approx 1.5$, $\epsilon^{48}\text{Ti} \approx 0$, and $\epsilon^{50}\text{Ti} \approx 9$), similar to considerations from Jordan et al. (2017) and Simon et al. (2017). However, this prediction remains only valid if input of ^{26}Al during the very early stages of the accretion disk was largely decoupled from significant changes in the Ti isotope abundances; an assumption that is difficult to reconcile with recent modeling of progressive changes in the protoplanetary disk during late infall (Nanne et al., 2019). Nevertheless, this proposed change in the isotopic nature of infalling material from the molecular cloud has intriguing consequences, as it could readily account for the evident isotope heterogeneity of CAIs in Ti (and in a few other elements), as well as for the less anomalous isotopic compositions in later formed Solar System materials (Brennecka et al., 2013).

6. CONCLUSIONS

1. The here investigated CAIs from CO and CM chondritic meteorites exhibit a certain degree of Ti isotope heterogeneity, similar to previously investigated large CAIs

from CV and CK meteorites (e.g., Davis et al., 2018; Torrano et al., 2017). This most likely reflects the heterogeneous distribution of at least one anomalous carrier phase among CAIs, conceivably induced through isotopic changes in the infalling cloud material.

2. Collectively, Ti isotope data reveal a close genetic relationship between regular CAIs (i.e., excluding FUN CAIs and hibonite-rich objects) from different carbonaceous chondrites (including CO, CM, CV, and CK meteorites) as well as to CAIs from ordinary chondrites (Ebert et al., 2018). This is suggestive of a close genetic relationship, most likely reflecting the fact that CAIs from various chondrite groups formed within a short timeframe, in a common region, and from similar matter.
3. The presence of closely affiliated refractory inclusions throughout various carbonaceous chondrite groups that accreted at distinct heliocentric distances provides evidence for large-scale transport of CAIs and may aid in placing constraints on early Solar System dynamics.
4. Two exceptional inclusions from Jbilet Winselwan—consisting largely of lath-shaped hibonite and/or spinel crystals—show highly anomalous and irregular nucleosynthetic Ti isotope signatures, which are clearly distinct to the population of regular CAIs. As such, these aggregates may represent an earlier generation of refractory material that formed prior to extensive homogenization of presolar matter. Further high-precision investigations of hibonite-rich objects and of inclusions similar to JW-4 and JW-7 may help in constraining the affiliation and chronological order of formation of these different types of refractory matter.

ACKNOWLEDGEMENTS

This work was supported by a Sofja Kovalevskaja Award from the Alexander von Humboldt Foundation to G.A.B. and DFG grant KL 1857/4 to T.K. Europlanet 2020 RI has received funding from the European Union's Horizon 2020 research and innovation program under grant agreement No. 654208. We thank U. Heitmann and E. S. Scherer for meteorite preparation and assistance with the Micromill, and T. Goral and S. S. Russell from the Natural History Museum, London, for sample characterization and fruitful discussions. The authors are appreciative of F. Moynier for editorial handling, and to A. M. Davis and two anonymous referees for their thoughtful comments that improved the manuscript.

APPENDIX A. SUPPLEMENTARY MATERIAL

Supplementary data to this article can be found online at <https://doi.org/10.1016/j.gca.2019.03.011>.

REFERENCES

Amari S., Nittler L. R., Zinner E., Lodders K. and Lewis R. S. (2001) Presolar SiC grains of Type A and B: their isotopic compositions and stellar origins. *Astrophys. J.* **559**, 463.

- Bischoff A., Ebert S., Metzler K. and Lentfort S. (2017) Breccia classification of CM chondrites. *Meteorit. Planet. Sci.* **52**, #6089.
- Braukmüller N., Wombacher F., Hezel D. C., Escoube R. and Münker C. (2018) The chemical composition of carbonaceous chondrites: Implications for volatile element depletion, complementarity and alteration. *Geochim. Cosmochim. Acta* **239**, 17–48.
- Brennecka G. A., Borg L. E. and Wadhwa M. (2013) Evidence for supernova injection into the solar nebula and the decoupling or r-process nucleosynthesis. *Proc. Nat. Acad. Sci.* **110**, 17241–17246.
- Brownlee D. et al. (2006) Comet 81P/Wild 2 under a microscope. *Science* **314**, 1711–1716.
- Burkhardt C., Kleine T., Oberli F., Pack A., Bourdon B. and Wieler R. (2011) Molybdenum isotope anomalies in meteorites: constraints on solar nebula evolution and origin of the Earth. *Earth Planet. Sci. Lett.* **312**, 390–400.
- Charlier B. L. A., Ginibre C., Morgan D., Nowell G. M., Pearson D. G., Davidson J. P. and Ottley C. J. (2006) Methods for the microsampling and high-precision analysis of strontium and rubidium isotopes at single crystal scale for petrological and geochronological applications. *Chem. Geol.* **232**, 114–133.
- Ciesla F. J. (2010) The distributions and ages of refractory objects in the solar nebula. *Icarus* **208**, 455–467.
- Clayton R. N. (2008) Oxygen isotopes in the early solar system – a Historical Perspective. *Rev. Mineral. Geochem.* **68**, 5–14.
- Connelly J. N., Bollard J. and Bizzarro M. (2017) Pb-Pb chronometry and the early solar system. *Geochim. Cosmochim. Acta* **201**, 345–363.
- Dauphas N., Chen J. H., Zhang J., Papanastassiou D. A., Davis A. M. and Travaglio C. (2014) Calcium-48 isotopic anomalies in bulk chondrites and achondrites: evidence for a uniform isotopic reservoir in the inner protoplanetary disk. *Earth Planet. Sci. Lett.* **407**, 96–108.
- Dauphas N. and Schauble E. A. (2016) Mass fractionation laws, mass-independent effects, and isotopic anomalies. *Annu. Rev. Earth Planet. Sci.* **44**, 709–783.
- Davis A. M., Zhang J., Greber N. D., Hu J., Tissot F. L. H. and Dauphas N. (2018) Titanium isotopes and rare earth patterns in CAIs: evidence for thermal processing and gas-dust decoupling in the protoplanetary disk. *Geochim. Cosmochim. Acta* **221**, 275–295.
- Desch S. J., Kalyaan A. and Alexander C. M. O'D. (2018) The effect of Jupiter's formation on the distribution of refractory elements and inclusions in meteorites. *Astrophys. J. Suppl. S.* **238**, 11.
- Ebert S., Render J., Brennecka G. A., Burkhardt C., Bischoff A., Gerber S. and Kleine T. (2018) Ti isotopic evidence for a non-CAI refractory component in the inner solar system. *Earth Planet. Sci. Lett.* **498**, 257–265.
- Friedrich J. M., Wang M.-S. and Lipschutz M. E. (2002) Comparison of the trace element composition of Tagish Lake with other primitive carbonaceous chondrites. *Met. Planet. Sci.* **37**, 677–686.
- Friend P., Hezel D. C., Barrat J.-A., Zipfel J., Palma H. and Metzler K. (2018) Composition, petrology, and chondrule-matrix complementarity of the recently discovered Jbilet Winselwan CM2 chondrite. *Meteorit. Planet. Sci.* **53**, 2470–2491.
- Gerber S., Burkhardt C., Budde G., Metzler K. and Kleine T. (2017a) Mixing and transport of dust in the early solar nebula as inferred from titanium isotope variations among chondrules. *Astrophys. J.* **841**, L17–L23.
- Greber N. D., Dauphas N., Puchtel I. S., Hofmann B. A. and Arndt N. T. (2017b) Titanium stable isotopic variations in chondrites, achondrites, and lunar rocks. *Geochim. Cosmochim. Acta* **213**, 534–552.
- Gyngard F., Amari S., Zinner E. and Marhas K. K. (2018) Correlated silicon and titanium isotopic compositions of presolar SiC grains from the Murchison CM2 chondrite. *Geochim. Cosmochim. Acta* **221**, 145–161.
- Ireland T. R. (1990) Presolar isotopic and chemical signatures in hibonite-bearing refractory inclusions from the Murchison carbonaceous chondrite. *Geochim. Cosmochim. Acta* **54**, 3219–3237.
- Itoh S., Kojima H. and Yurimoto H. (2004) Petrography and oxygen isotopic compositions in refractory inclusions from CO chondrites. *Geochim. Cosmochim. Acta* **68**, 183–194.
- Jacobsen B., Yin Q.-Z., Moynier F., Amelin Y., Krot A. N., Nagashima K., Hutcheon I. D. and Palme H. (2008) ^{26}Al - ^{26}Mg and ^{207}Pb - ^{206}Pb systematics of Allende CAIs: canonical solar initial $^{26}\text{Al}/^{27}\text{Al}$ ratio reinstated. *Earth Planet. Sci. Lett.* **272**, 353–364.
- Jacobsen B., Han J. M., Matzel J. E., Brearley A. J. and Hutcheon I. D. (2014) Oxygen isotopes in fine-grained spinel-pyroxene and melilite-rich CAIs in the ALHA 77307 CO3.0 carbonaceous chondrite. *Lunar Planet. Sci.* **45**, #2789.
- Jordan M. K., Kohl I. E., McCain K. A., Simon J. I. and Young E. D. (2017) Ti isotopes: echoes of grain-scale heterogeneity in the protoplanetary disk. *Lunar Planet. Sci.* **48**, #3032.
- Kööp L., Davis A. M., Nakashima D., Park C., Krot A. N., Nagashima K., Tenner T. J., Heck P. R. and Kita N. T. (2016a) A link between oxygen, calcium and titanium isotopes in ^{26}Al -poor hibonite-rich CAIs from Murchison and implications for the heterogeneity of dust reservoirs in the solar nebula. *Geochim. Cosmochim. Acta* **189**, 70–95.
- Kööp L., Nakashima D., Heck P. R., Kita N. T., Tenner T. J., Krot A. N., Nagashima K., Park C. and Davis A. M. (2016b) New constraints on the relationship between ^{26}Al and oxygen, calcium, and titanium isotopic variation in the early Solar System from a multielement isotopic study of spinel-hibonite inclusions. *Geochim. Cosmochim. Acta* **184**, 151–172.
- Kööp L., Davis A. M., Krot A. N., Nagashima K. and Simon S. B. (2018a) Calcium and titanium isotopes in refractory inclusions from CM, CO and CR chondrites. *Earth Planet. Sci. Lett.* **489**, 179–190.
- Kööp L., Nakashima D., Heck P. R., Kita N. T., Tenner T. J., Krot A. N., Nagashima K., Park C. and Davis A. M. (2018b) A multielement isotopic study of refractory FUN and F CAIs: mass-dependent and mass-independent isotope effects. *Geochim. Cosmochim. Acta* **221**, 296–317.
- Kornacki A. S. and Wood J. A. (1984) Petrography and Classification of Ca, Al-rich and Olivine-rich inclusions in the Allende CV3 chondrite. *J. Geophys. Res.* **89**, B573–B587.
- Krot A. N., Nagashima K., Ciesla F. J., Meyer B. S., Hutcheon I. D., Davis A. M., Huss G. R. and Scott E. R. D. (2010) Oxygen isotopic composition of the protosolar silicate dust: Evidence from refractory inclusions. *Astrophys. J.* **713**, 1159–1166.
- Kruijer T. S., Kleine T., Fischer-Gödde M., Burkhardt C. and Wieler R. (2014) Nucleosynthetic W isotope anomalies and the Hf-W chronometry of Ca–Al-rich inclusions. *Earth Planet. Sci. Lett.* **403**, 317–327.
- Larsen K. K., Trinquier A., Paton C., Schiller M., Wielandt D., Ivanova M. A., Connelly J. N., Nordlund Å., Krot A. N. and Bizzarro M. (2011) Evidence for magnesium isotope heterogeneity in the solar protoplanetary disk. *Astrophys. J.* **735**, L37–L43.
- Larsen K. K., Wielandt D. and Bizzarro M. (2018) Multi-element ion-exchange chromatography and high-precision MC-ICP-MS

- isotope analysis of Mg and Ti from sub-mm-sized meteorite inclusions. *J. Anal. At. Spectrom.* **33**, 613–628.
- Lee M. R. and Greenwood R. C. (1994) Alteration of calcium- and aluminium-rich inclusions in the Murray (CM2) carbonaceous chondrite. *Meteoritics* **29**, 780–790.
- Leya I., Schönbächler M., Krähennühl U. and Halliday A. N. (2009) New titanium isotope data for Allende and Efremovka CAIs. *Astrophys. J.* **702**, 1118–1126.
- Liu M.-C., McKeegan K. D., Goswami J. N., Marhas K. K., Sahijpal S., Ireland T. R. and Davis A. M. (2009) Isotopic records in CM hibonites: implications for timescales of mixing of isotope reservoirs in the solar nebula. *Geochim. Cosmochim. Acta* **73**, 5051–5079.
- Matzel J. E. P. et al. (2010) Constraints on the formation age of cometary material from the NASA Stardust mission. *Science* **328**, 483–486.
- Matzel J. E. P., Simon J. I., Hutcheon I. D., Jacobsen B., Simon S. B. and Grossman L. (2013) Oxygen isotope measurements of a rare Murchison type A CAI and its rim. *Lunar Planet. Sci.* **44**, #2632.
- McKeegan K. D., Leshin L. A., Russell S. S. and MacPherson G. J. (1998) Oxygen isotopic abundances in calcium-aluminum-rich inclusions from ordinary chondrites: implications for nebular heterogeneity. *Science* **280**, 414–417.
- McKeegan K. D. et al. (2006) Isotopic compositions of cometary matter returned by stardust. *Science* **314**, 1724–1728.
- Myojo K., Yokoyama T., Okabayashi S., Wakaki S., Sugiura N. and Iwamori H. (2018) The origin and evolution of nucleosynthetic Sr isotope variability in calcium and aluminum-rich refractory inclusions. *Astrophys. J.* **853**, 48.
- Nanne J. A. M., Nimmo F., Cuzzi J. N. and Kleine T. (2019) Origin of the non-carbonaceous-carbonaceous meteorite dichotomy. *Earth Planet. Sci. Lett.* **511**, 44–54.
- Niederer F. R., Papanastassiou D. A. and Wasserburg G. J. (1981) The isotopic composition of titanium in the Allende and Leoville meteorites. *Geochim. Cosmochim. Acta* **45**, 1017–1031.
- Niemeyer S. (1988) Titanium isotopic anomalies in chondrules from carbonaceous chondrites. *Geochim. Cosmochim. Acta* **52**, 309–318.
- Niemeyer S. and Lugmair G. W. (1981) Ubiquitous isotopic anomalies in Ti from normal Allende inclusions. *Earth Planet. Sci. Lett.* **53**, 211–225.
- Park C., Nagashima K., Wasserburg G. J., Papanastassiou D. A., Hutcheon I. D., Davis A. M., Huss G. R., Bizzarro M. and Krot A. N. (2014) Calcium and Titanium isotopic compositions of FUN CAIs: implications for their origin. *Lunar Planet. Sci.* **45**, #2656.
- Render J., Fischer-Gödde M., Burkhardt C. and Kleine T. (2017) The cosmic molybdenum-neodymium isotope correlation and the building material of the Earth. *Geochim. Persp. Lett.* **3**, 170–178.
- Render J., Brennecka G. A., Wang S.-J., Wasylenki L. E. and Kleine T. (2018) A distinct nucleosynthetic heritage for early solar system solids recorded by Ni isotope signatures. *Astrophys. J.* **862**, 26–43.
- Russell S. S., Srinivasan G., Huss G. R., Wasserburg G. J. and MacPherson G. J. (1996) Evidence for widespread ^{26}Al in the solar nebula and constraints for nebula time scales. *Science* **273**, 757–762.
- Shollenberger Q. R., Borg L. E., Render J., Ebert S., Bischoff A., Russell S. S. and Brennecka G. A. (2018a) Evidence for isotopic homogeneity in the CV/CK CAI-forming region inferred from multiple isotope systems in refractory inclusions. *Geochim. Cosmochim. Acta* **228**, 62–80.
- Shollenberger Q. R., Render J. and Brennecka G. A. (2018b) Er, Yb, and Hf isotopic compositions of refractory inclusions: an integrated isotopic fingerprint of the Solar System's earliest reservoir. *Earth Planet. Sci. Lett.* **495**, 12–23.
- Simon J. I., Jordan M. K., Tappa M. J., Schauble E. A., Kohl I. E. and Young E. D. (2017) Calcium and titanium isotope fractionation in refractory inclusions: tracers of condensation and inheritance in the early solar protoplanetary disk. *Earth Planet. Sci. Lett.* **472**, 277–288.
- Simon S. B. et al. (2008) A refractory inclusion returned by Stardust from comet 81P/Wild 2. *Meteorit. Planet. Sci.* **43**, 1861–1877.
- Simon S. B., Krot A. N., Nagashima K., Kööp L. and Davis A. M. (2019) Condensate refractory inclusions from the CO3.00 chondrite Dominion Range 08006: petrography, mineral chemistry, and isotopic compositions. *Geochim. Cosmochim. Acta* **246**, 109–122.
- Torrano Z. A., Rai V. K. and Wadhwa M. (2017) Magnesium, Titanium and Chromium isotope compositions of refractory inclusions from several CV3 and CK3 chondrites: Implications for nebular heterogeneity. *Lunar Planet. Sci.* **48**, #3045.
- Trinquier A., Elliott T., Ulfbeck D., Coath C., Krot A. N. and Bizzarro M. (2009) Origin of nucleosynthetic isotope heterogeneity in the solar protoplanetary disk. *Science* **324**, 374–376.
- Ushikubo T., Jenner T. J., Hiyagon H. and Kita N. T. (2017) A long duration of the ^{16}O -rich reservoir in the solar nebula, as recorded in fine-grained refractory inclusions from the least metamorphosed carbonaceous chondrites. *Geochim. Cosmochim. Acta* **201**, 103–122.
- Wanajo S., Janka H.-T. and Müller B. (2013) Electron-capture supernovae as origin of ^{48}Ca . *Astrophys. J.* **767**, L26–L31.
- Warren P. (2011) Stable-isotopic anomalies and the accretionary assemblage of the Earth and Mars: a subordinate role for carbonaceous chondrites. *Earth Planet. Sci. Lett.* **311**, 93–100.
- Wasserburg G. J., Wimpenny J. and Yin Q.-Z. (2012) Mg isotopic heterogeneity, Al-Mg isochrons, and canonical $^{26}\text{Al}/^{27}\text{Al}$ in the early solar system. *Meteorit. Planet. Sci.* **47**, 1980–1997.
- Wasserburg G. J., Trippella O. and Busso M. (2015) Isotope anomalies in the Fe-group elements in meteorites and connections to nucleosynthesis in AGB stars. *Astrophys. J.* **805**, 7–25.
- Wasson J. T., Yurimoto H. and Russell S. S. (2001) ^{16}O -rich melilite in CO3.0 chondrites: possible formation of common, ^{16}O -poor melilite by aqueous alteration. *Geochim. Cosmochim. Acta* **65**, 4539–4549.
- Williams C. D., Janney P. E., Hines R. R. and Wadhwa M. (2016) Precise titanium isotope compositions of refractory inclusions in the Allende CV3 chondrite by LA-MC-ICPMS. *Chem. Geol.* **436**, 1–10.
- Wood J. A. (2005) The chondrite types and their origins. In *Chondrites and the Protoplanetary Disk* (eds. A. N. Krot, E. R. D. Scott and B. Reipurth), Proc. Astron. Soc. Pacific Conf. Series, pp. 953–971.
- Yang L. and Ciesla F. J. (2012) The effects of disk building on the distributions of refractory materials in the solar nebula. *Meteorit. Planet. Sci.* **47**, 99–119.
- Zhang J., Dauphas N., Davis A. M. and Pourmand A. (2011) A new method for MC-ICPMS measurement of titanium isotopic composition: identification of correlated isotope anomalies in meteorites. *J. Anal. At. Spectrom.* **26**, 2197–2205.